processes

MDPI

Article

Catalytic Biomass Transformation to Hydrocarbons under Supercritical Conditions over Nickel Supported on Schungite

Elena O. Schipanskaya [1], Antonina A. Stepacheva [2], Mariia E. Markova [2], Alexey V. Bykov [2], Alexander I. Sidorov [2], Valentina G. Matveeva [1,2], Mikhail G. Sulman [2] and Lioubov Kiwi-Minsker [2,3,*]

1 Regional Technological Center, Tver State University, Zhelyabova Str., 33, 170100 Tver, Russia; bliznjshka@bk.ru (E.O.S.); matveeva@science.tver.ru (V.G.M.)
2 Department of Biotechnology, Chemistry and Standardization, Tver State Technical University, A. Nikitin Str., 22, 170026 Tver, Russia; a.a.stepacheva@mail.ru (A.A.S.); mashulikmarkova@gmail.com (M.E.M.); bykovav@yandex.ru (A.V.B.); sidorov_science@mail.ru (A.I.S.); sulmanmikhail@yandex.ru (M.G.S.)
3 Institute of Chemical Sciences and Engineering, Ecole Polytechnique Fédérale de Lausanne, CH-1015 Lausanne, Switzerland
* Correspondence: lioubov.kiwi-minsker@epfl.ch; Tel.: +41-76-334-0861

Abstract: Liquid fuel production from biomass-derived molecules has received great attention due to the diminished fossil fuel reserves, growing energy demand, and the necessity of CO_2 emission reduction. The deoxygenation of oils and fatty acids is a promising process to obtain "green" diesel. Herein, we report the results of the study of the deoxygenation of stearic acid to alkanes as a model reaction. Series of Ni-supported on schungite were obtained by precipitation in subcritical water (hydrothermal deposition) and for comparison via wetness impregnation followed, in both cases, by calcination at 500 °C and a reduction in H_2 at 300 °C. The catalyst obtained via hydrothermal synthesis showed a three-fold higher specific surface area with a four-fold higher active phase dispersion compared to the catalysts synthesized via conventional impregnation. The catalysts were tested in stearic acid deoxygenation in supercritical n-hexane as the solvent. Under optimized process conditions (temperature of 280 °C, hydrogen partial pressure of 1.5 MPa, and 13.2 mol of stearic acid per mol of Ni), a close to 100% yield of C_{10}–C_{18} alkanes, containing over 70 wt.% of targeted n-heptadecane, was obtained after 60 min of reaction.

Keywords: deoxygenation; green diesel; stearic acid; schungite support; Ni-catalyst

Citation: Schipanskaya, E.O.; Stepacheva, A.A.; Markova, M.E.; Bykov, A.V.; Sidorov, A.I.; Matveeva, V.G.; Sulman, M.G.; Kiwi-Minsker, L. Catalytic Biomass Transformation to Hydrocarbons under Supercritical Conditions over Nickel Supported on Schungite. *Processes* **2024**, *12*, 1503. https://doi.org/10.3390/pr12071503

Academic Editor: Cunshan Zhou

Received: 5 June 2024
Revised: 6 July 2024
Accepted: 14 July 2024
Published: 17 July 2024

1. Introduction

The production of liquid fuels from alternative sources is of great importance in view of sustainability issues. Among the existing fuels-from-biomass, green diesel is considered to be the most prospective [1–3] as its composition and properties are close to the diesel fuel obtained from fossil sources. Moreover, green diesel has multiple advantages like carbon neutrality and higher cetane number, and it can be produced from greases, as well as non-edible and waste cooking oils [3–8].

The production of green diesel is performed usually at relatively high temperatures (250–450 °C) under hydrogen pressure of 0.5–5.0 MPa, where different reactions take place: decarbonylation [2,9], decarboxylation [4,9], deoxygenation [10,11], hydrogenation [5,9], hydrogenolysis [2], and cracking [4,10]. In the undesired processes, fatty acids and triglycerides, as well as their derivatives (i.e., fatty acid esters), are decomposed to the thermodynamically stable CO, CO_2, and H_2O. The efficiency of green diesel production strongly depends on the catalyst, presence/absence of solvent, and gaseous atmosphere. The use of a solvent is preferable to avoid mass transfer limitations due to the high viscosity of triglycerides. Among the solvents, high-boiled hydrocarbons such as decane [5,8,9], dodecane [2,4,5,12], and tetradecane [13] are often applied. However, such a process requires high temperature and high hydrogen pressure caused by the low hydrogen solubility in

the reaction mixture. In recent years, interest has grown to include solvents in sub- and supercritical states for green diesel production [14–18]. Sub- or supercritical water has been reported for the deoxygenation of triglycerides, fatty acids, and their esters [19–24]. The use of supercritical solvent reduces the mass transfer limitations due to the formation of the reaction mixture in a pseudo-homogeneous phase. This substantially increases the reaction rate, diminishing the process duration. However, water has a relatively high critical point, resulting in a high process temperature. Moreover, supercritical water can be aggressive for the materials used in deoxygenation. Thus, the search for a supercritical solvent, which is characterized by a lower critical temperature in comparison with water, easy separation from the reaction mixture, and high solubility of hydrogen and organic compounds, is warranted.

For the conversion of fatty acids and their derivatives, different metals and oxides are applied as effective catalysts. The use of Pd [14,16–19], Pt [16–19], Ru [14,16–20], Re [16–18], Ni [7,9,13,15,21–23], and Co [9,21,24,25] has been reported for several decades. In the metallic form, they effectively catalyze decarbonylation and decarboxylation in a hydrogen atmosphere. The use of Ni, Co, and Mo oxides [5,22]; sulfides [7,13]; and phosphides [8,24] in the deoxygenation of fatty acids has also been investigated. Among the catalytic supports, Al_2O_3 [16,18,26], SiO_2 [8,15,27], zeolites [11,18,23,27–29], ZrO_2 [16,18,26], porous organic frameworks [16,18,28], activated carbon/carbonaceous materials [7,14,17,19,20,22,24,25], and TiO_2 [10,16] are reported.

The main issue of deoxygenation is its high cost, where reduction can be achieved by carrying out the process under supercritical conditions at a lower temperature over an effective catalyst. The cost of catalysts containing noble metals is also an issue. The application of transition metals instead of noble ones, supported on unexpensive porous materials, could overcome this issue if the catalyst demonstrates a high activity and stability.

In this work, a natural unexpensive carbonaceous material, schungite, was used as a support. The schungite composite consists of an amorphous fullerene-like carbon matrix with uniformly distributed highly dispersed inorganic crystals. Besides carbon, schungite contains silicon, aluminium, titan, and iron oxides, as well as the oxides of alkali and alkali-earth metals. It is characterized by a high electro and thermal conductivity and mechanical strength, and has a high adhesion/adsorption capacity towards fatty acids [30–34], and is a potentially suitable support for catalyst preparation [34,35]. However, schungite catalysts prepared via wetness impregnation were not efficient due to the relatively low specific surface area because of the pore blockage by the formed metal particles. Therefore, we synthesized catalysts through precipitation in subcritical water. This method of active phase deposition was shown to maintain the specific surface area and porosity of the pristine support.

Herein, we report the results on stearic acid (model of fatty acids) deoxygenation in the supercritical solvent (n-hexane) over novel Ni/schungite catalysts prepared via hydrothermal synthesis. The catalysts were thoroughly characterized by physico-chemical methods. The main kinetic parameters (reaction rate, partial orders, and apparent activation energy), and optimal process conditions were also reported.

2. Materials and Methods

2.1. Materials

Stearic acid (99.9%) was purchased from Khimmedservice (Moscow, Russia) and was used without additional purification. n-Hexane (99%, Reachim, Moscow, Russia) was used as the solvent. Hydrogen (99.9%, GasProduct, Tver, Russia) was used for deoxygenation.

For the catalyst synthesis, schungite was purchased from Schungite Export (Petrozavodsk, Russia). Its characteristics are as follows: carbon content of 20 wt.%; ash content of 75 wt.%; packed density of 450 g/dm^3; moisture content of 2.5 wt.%; specific surface area (SSA) of 17 m^2/g; particle size between 0.1–0.2 µm. Nickel nitrate hexahydrate, nickel acetate, and nickel chloride (Aurat, Moscow, Russia) dissolved in distilled water were used as the precursors of the active phase.

2.2. Schungite-Based Catalyst Preparation

The catalysts were prepared by two methods: incipient wetness impregnation and precipitation in the subcritical water. The impregnation was carried out according to the following procedure (see Figure S1): 2 g of the schungite was mixed at 50 °C for 30 min with a solution containing 5 mL of distilled water and the calculated amount of the nickel precursor. The weight of the nickel salt was calculated to obtain the Ni concentration in the catalysts of 2, 5, and 10 wt.%. The resulting suspension was dried at 100 ± 5 °C on air overnight. The dry sample was calcinated in air at 500 °C for 5 h and reduced in a quartz tube with hydrogen flow at 300 °C for 3 h. The obtained samples were designated as Ni/Schungite-WI.

The catalyst synthesis through precipitation in subcritical water (hydrothermal synthesis) was carried out in a stainless-steel autoclave PARR 4307 (Parr Instrument Ltd., Moline, IN, USA) (see Figure S2). The catalyst synthesis was carried out according to the following procedure (Figure S3): 2 g of schungite, a pre-calculated amount of nickel precursor salt, and 15 mL of distilled water were put into the reactor cell with a volume of 25 mL. The mixture was heated up to 200 °C under nitrogen pressure of 4.0 MPa at a constant stirring at the rate of 700 rpm. After attaining the synthesis temperature, the mixture was maintained for 15 min at constant stirring. Then, the reactor was cooled down to room temperature, the reaction mixture was filtered, and the sample was dried at 100 ± 5 °C overnight. Then, the catalyst was calcinated in air at 500 °C for 5 h and reduced in a quartz tube with hydrogen flow at 300 °C for 3 h. The samples were designated as Ni/Schungite-SCW.

2.3. Catalyst Characterization

The specific surface area, porosity, and pore size distribution of the samples were determined by nitrogen low-temperature adsorption using a Beckman Coulter SA 3100 (Coulter Corporation, Brea, CA, USA) analyzer. Before the analysis, the samples were outgassed in the Beckmann Coulter SA-PREP (Coulter Corporation, Brea, CA, USA) at 120 °C in a vacuum for 1 h. To calculate the specific surface area and total pore volume, the Brunauer–Emmet–Teller model was applied. Pore size distribution was evaluated using the Harkins–Jure equation.

X-ray powder diffraction (XRD) patterns were collected on an Empyrean from PANalytical (Malvern, UK). X-rays were generated from a copper target with a scattering wavelength of 1.54 Å. The step size was 0.02.

The thermogravimetric analysis of the samples was carried out via TG 209 F1 YRIS (Netzsch, Zelb, Germany). Argon (high purity) was used as a medium. The analysis was performed according to the following temperature program: 30 °C (5 min) → 10 K/min (600 °C) → 600 °C (10 min). Active argon flow through the furnace of thermal weights was 20 mL/min, and the protective flow rate was maintained at 20 mL/min during the analysis.

The H_2-TPR study was carried out in an AutoChem HP (Micromeritics Ltd., Norcross, GA, USA) using a U-tube quartz reactor. The analysis was performed at a temperature range of 30–600 °C with a heating rate of 5 °C/min and was then kept at 600 °C for 1 h. The reductive atmosphere contained 10 vol. % H_2 in Ar. The gas flow rate was 30 mL/min. The quantity of the desorbed gas was determined using calibration curves.

The transmission electron microscopy (TEM) study of the catalysts was performed using a JEOL JEM1010 scanning transmission electron microscope (Jeol Ltd., Tokyo, Japan) operating at 80 kV. The samples were embedded in an epoxy resin and microtomed in cross sections (ca. 100 nm thick). Images of the resulting sections were collected with a Gatan digital camera (Gatan Inc., Pleasanton, CA, USA) and they were analyzed with the Adobe Photoshop v.22.0.0 software package and the Scion Image Processing Toolkit v.4.0.

2.4. Deoxygenation Procedure

Stearic acid deoxygenation was carried out in a stainless-steel batch reactor Parr 5000 Multiple Reactor System (Parr Instrument Ltd., Moline, IN, USA) (see Figure S4) equipped with a magnetic stirrer. The volume of the reactor cell was 50 mL. For each

experiment, a solution of the stearic acid in n-hexane with a concentration of 33 g/L, and a weighted amount of the Ni-catalyst were placed into the reactor cell. The reactor was sealed and purged with nitrogen to remove the air. The reaction mixture was heated up to the operation temperature in hydrogen atmosphere. The temperature was varied from 240 up to 300 °C. The partial pressure of hydrogen varied from 0.5 up to 3.0 MPa. The deoxygenation was carried out at constant stirring of 1200 rpm. Samples (10 μL) of the liquid phase were collected every 10 min through the capillary sampler allowing for maintaing the system equilibrium.

2.5. Liquid Phase Analysis

The analysis of liquid phase was performed by GCMS using a gas chromatograph GC-2010 and mass-spectrometer GCMS-QP2010S (Shimadzu, Kyoto, Japan) equipped with chromatographic column HP-1MS (length of 30 m, diameter of 0.25 mm, and film thickness of 0.25 μm). The analysis was carried out under the following conditions: an initial temperature of 120 °C was maintained for 5 min, then the column was heated up to 250 °C at a rate of 5 °C/min and it was maintained at 250 °C for 5 min. Helium (flow rate of 20.8 mL/s, pressure of 253.5 kPa) was used as a carrier gas. The injector temperature was 280 °C, the ion source temperature was 260 °C and the interface temperature was 280 °C. Methylene diamine was used as an external standard for quantitative determination. For the proper quantitative determination, calibrations regarding the main compounds—stearic acid and n-heptadecane—were performed.

3. Results and Discussion

3.1. Catalyst Characterization

The schungite used in this work was an inexpensive support suitable for catalyst preparation. The incipient wetness impregnation (WI) and the precipitation in the sub-critical water (SCW) were used to obtain 5 wt.% Ni-containing catalysts with the nickel nitrate as a precursor. The catalysts were designated as 5%-Ni/schungite-WI and 5%-Ni/schungite-SCW, respectively. The specific surface area, surface composition, and Ni dispersion were compared. The characteristics of these catalysts are presented in Table 1.

Table 1. Characteristics of the catalysts.

Sample	Pore Volume, cm^3/g	Specific Surface Area, m^2/g *	Ni Concentration, wt.% **	Ni Particle Mean Diameter, nm	Ni Dispersion, % ***
Schungite	0.06 ± 0.01	22 ± 2	-	-	-
Schungite calcinated	0.06 ± 0.01	29 ± 2	-	-	-
5%-Ni/schungite-WI	0.05 ± 0.01	10 ± 1	3.2 ± 0.1	12.2 ± 0.1	8.8 ± 0.2
5%-Ni/schungite-WI calcinated	0.06 ± 0.01	27 ± 2	3.2 ± 0.1	13.7 ± 0.2	7.9 ± 0.1
5%-Ni/schungite-WI reduced	0.05 ± 0.01	17 ± 1	3.2 ± 0.1	15.4 ± 0.2	6.8 ± 0.1
5%-Ni/schungite-SCW	0.08 ± 0.01	34 ± 3	4.9 ± 0.1	4.2 ± 0.1	23.4 ± 0.2
5%-Ni/schungite-SCW calcinated	0.16 ± 0.02	69 ± 3	4.9 ± 0.1	4.5 ± 0.1	22.9 ± 0.2
5%-Ni/schungite-SCW reduced	0.15 ± 0.02	61 ± 2	4.9 ± 0.1	4.6 ± 0.1	21.3 ± 0.2

* According to the BET model. ** Ni concentration was estimated by the X-ray fluorescence analysis. *** Ni dispersion was estimated according to CO chemisorption analysis.

The analysis of the catalysts by the low-temperature nitrogen physisorption showed that while the catalyst was prepared by the wetness impregnation, a two-fold decrease in the specific surface area was observed (Table 1). The calcination of the sample led to

the surface area recovering because of the evaporation of the solvent adsorbed and the formation of Ni-containing phase crystals. For the method of precipitation in subcritical water, an increase in the specific surface area by 1.5 times was observed for the sample compared with the as-received support. Such an increase can be explained by the partial removal of schungite components in subcritical water, like the dissolution of alkali and alkali-earth metal oxides during the hydrothermal synthesis forming supplemental pores, as well as the recrystallization of the silicon and aluminum oxides, as shown below by the XRD study. This was also confirmed by the elemental composition of the schungite that changed after the treatment under the catalyst synthesis conditions (see Table 2) [36]. The calcination of the sample led to an increase in the surface area by more than three times in comparison with the initial schungite support. The reduction in samples was found to lead to a decrease in the specific surface area, probably due to the slight increase in Ni-particle size (see Table 1).

Table 2. Alkali and alkali-earth metal concentrations in schungite.

Element	Concentration, wt.% *	
	Initial	After Treatment in Subcritical Water
Ba	0.32 ± 0.01	0.15 ± 0.01
Ca	0.09 ± 0.01	0.02 ± 0.01
Mg	0.34 ± 0.01	0.12 ± 0.01
K	1.02 ± 0.01	0.08 ± 0.01
Na	0.27 ± 0.01	0.06 ± 0.01

* According to the X-ray fluorescence analysis.

It should be noted that the porous structure of the support material was maintained during both the WI and SCW methods, as shown by the nitrogen adsorption–desorption isotherms (see Figure 1a,b). The forms of isotherms were similar for all of the samples studied and can be attributed to type IV with a hysteresis loop of the H4 type. The H4 type with a narrow hysteresis loop, the adsorption curve, and the desorption curve gradually ascend as the relative pressure becomes high. Adsorption saturation occurred when the balance pressure was close to the saturated vapor pressure, which usually indicates that the pore shape was silt-pore (micro-pore). Also, this type of isotherm was a characteristic of meso/micro-porous materials with strong adsorbate–adsorbent interactions and a broad pore size distribution (see Figure 1c) [37]. From Figure 1c, it follows that catalyst synthesis by the WI method led to a decrease in small pores and an increase in the large pore relative content, probably due to pore blockage by the Ni precursor and the adsorbed water. The catalyst synthesis by the SCW method did not lead to changes in the pore size distribution, preserving the porous structure of the support.

The XRD patterns of the initial schungite and the synthesized catalysts are presented in Figure 2. The analysis showed the presence of amorphous carbon (JCPDS 026-1080), α-SiO_2 (JCPDS 086-1628), β-SiO_2 (JCPDS 084-0384), α-Al_2O_3 (JCPDS 089-7717), γ-Al_2O_3 (JCPDS 011-0517), and Fe_2O_3 (JCPDS 085-0987) in all of the samples (see Figure 2, line a). Other components of schungite were not observed by XRD due to their low concentration. When the catalyst was synthesized by WI, the position and intensity of the peak's characteristic of the initial schungite remained unchanged (see Figure 2, lines b and c). For the catalyst synthesized by the hydrothermal method, the intensity of peaks corresponding to α-Al_2O_3, γ-Al_2O_3, and β-SiO_2 changed, indicating the recrystallization of oxides during the synthesis (see Figure 2, lines d and e). For the samples obtained after calcination, the presence of peaks characteristic for β-NiO were observed in the XRD patterns at 2θ of ca. 37°, 43°, and 63° according to JCPDS card 47-1049. The reduction in samples led to the appearance of peaks corresponding to metallic Ni (JCDPS 04-0850) with 2θ of ca. 41°, 44°, and 52° [38,39]. It should be noted that the intensity of peaks characteristic of the metallic phase of Ni was found to be higher for the catalyst obtained by the precipitation in subcritical water.

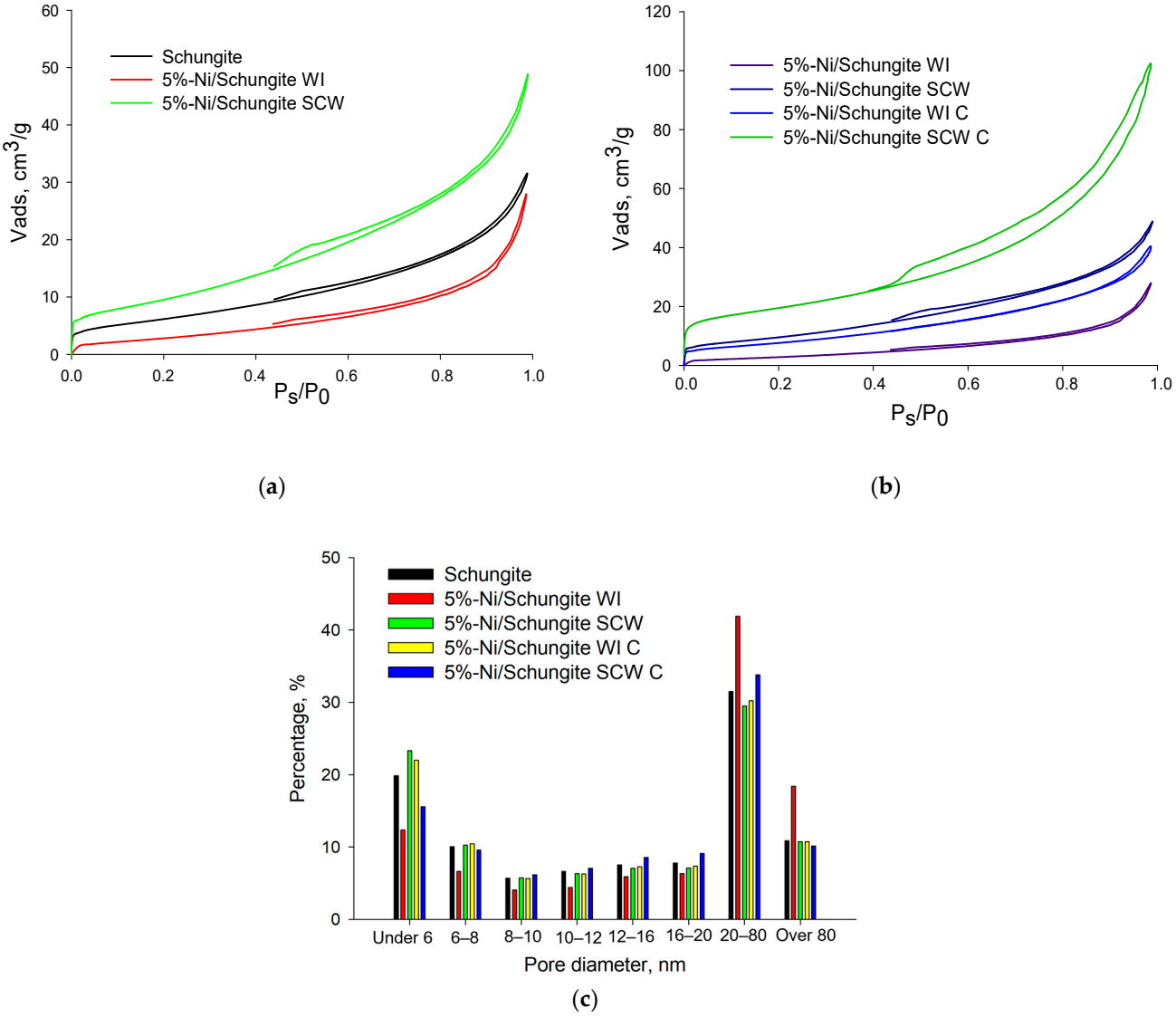

Figure 1. (**a**) Nitrogen adsorption–desorption isotherms for initial schungite and Ni-containing catalysts prepared by two methods; (**b**) nitrogen adsorption–desorption isotherms for as-prepared and calcinated catalysts; and (**c**) pore size distribution of the catalysts.

The thermogravimetric analysis of the samples obtained by both methods was carried out in a temperature range of 30–600 °C, which was chosen according to the temperatures of the catalyst synthesis (calcination and reduction) and testing in the reaction. Figure 3 presents the TG (a) and DTG (b) data. The thermograms of the initial schungite (line a) and calcinated 5%-Ni/schungite-SCW (line d) were close to each other. Slight differences were observed in the temperature range of 100–150 °C, which was explained by the sample humidity. For the sample synthesized by the precipitation in subcritical water (line c), the weight loss was higher than for the initial schungite. The first range of weight loss (at 100–150 °C) corresponded to the water evaporation. The ranges at 190–220 °C, 340–380 °C, and 460–520 °C corresponded to the decomposition of $Ni(OH)_2$, $Ni(OH)_3$, and NiOOH formed during the synthesis, as it has been shown previously [40,41]. The sample synthesized by the wetness impregnation was significantly different from the other samples. The thermogram for the as prepared 5%-Ni/schungite-WI was characterized by four ranges of weight loss—100–150 °C, 190–220 °C, 260–320 °C, and 460–520 °C—corresponding to the water evaporation and decomposition of $Ni(OH)_2$, $Ni(NO_3)_2$, and NiOOH, respectively. Based on the data of the thermogravimetric analysis, the thermal stability of the schungite

in the temperature range of 30–600 °C was confirmed. The absence of substantial changes in the schungite structure was also demonstrated by the FTIR spectra (see Figure S5).

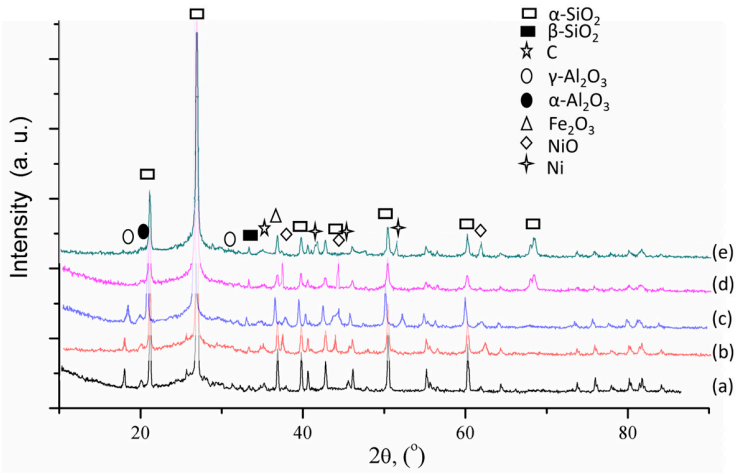

Figure 2. XRD patterns of schungite (a), calcinated 5%-Ni/schungite-WI (b), reduced 5%-Ni/schungite-WI (c), calcinated 5%-Ni/schungite-SCW (d), and reduced 5%-Ni/schungite-SCW (e).

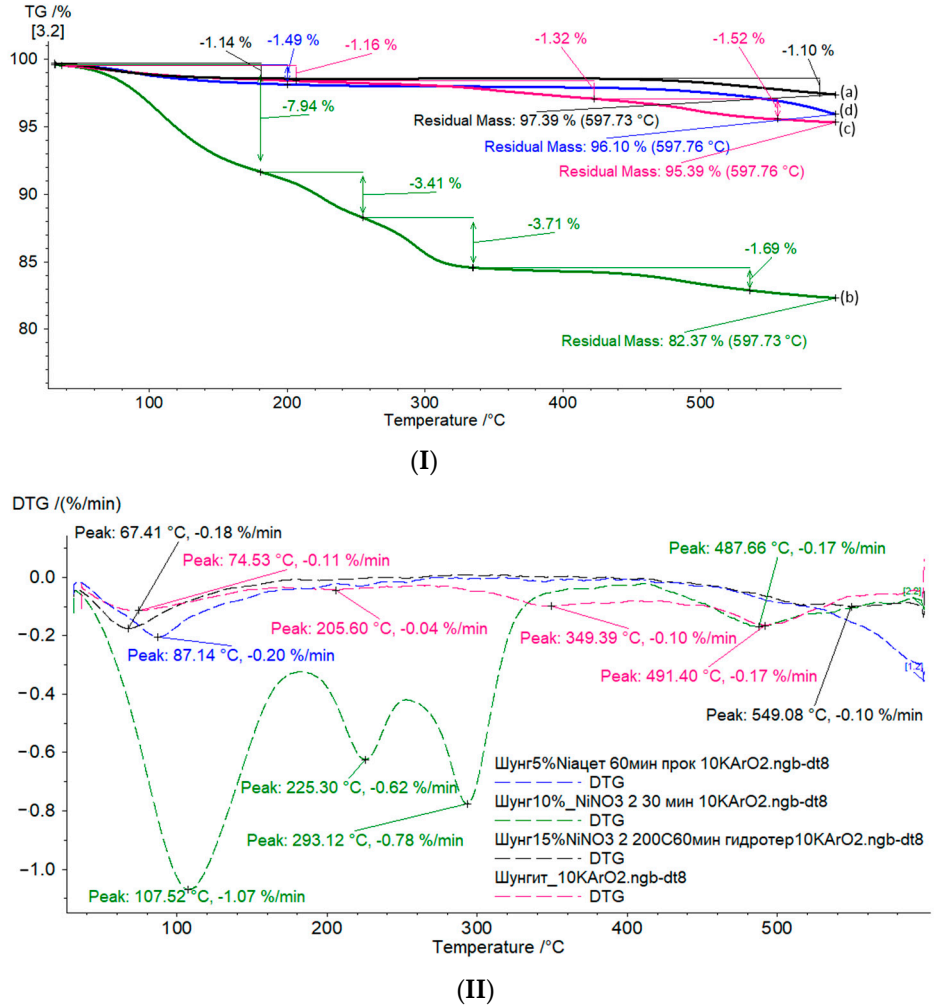

Figure 3. TD (**I**) and DTG (**II**) curves: schungite as received (a), 5%-Ni/schungite-WI as prepared (b), 5%-Ni/schungite-SCW as prepared (c), and 5%-Ni/schungite-SCW after calcination (d).

Th eTPR profiles of the synthesized catalysts are presented in Figure 4. For both catalysts, the partial reduction in the NiO phase started at 200 °C. In the TPR profile of catalysts synthesized by the WI method, a broad peak could be divided into four parts at ca. 250, 330, 370, and 450 °C, corresponding to the reduction in well-crystallized NiO particles [39,42]. The main NiO reduction region was found to be 330–370 °C. The first range in the reduction temperature (with a maximum at 250 °C) could be attributed to the NiO species weakly interacting with the support. However, according to the literature, the reduction in the Ni-containing monometallic catalyst was in the region between 350–700 °C [38,39,42–44]. Such a decrease in the reduction temperature of our catalysts could be due to the presence of transition metal oxides in schungite, which could serve as promoters for the reduction of the nickel oxide active phase. For the catalyst synthesized by the SCW method, two regions at ca. 300, and 360 °C were well observed, indicating a decrease in the reduction temperature in comparison with 5%-Ni/schungite-WI. This effect can be explained by the lower size of the nickel oxide particles that followed from the TEM images (see Figure 5).

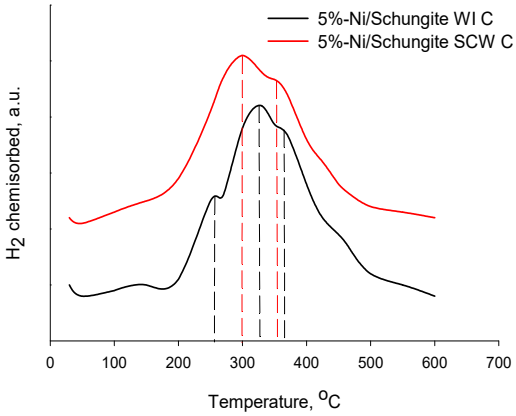

Figure 4. TPR profiles of the synthesized catalysts. Dashed lines indicate the temperatures of maximum H_2 chemisorption.

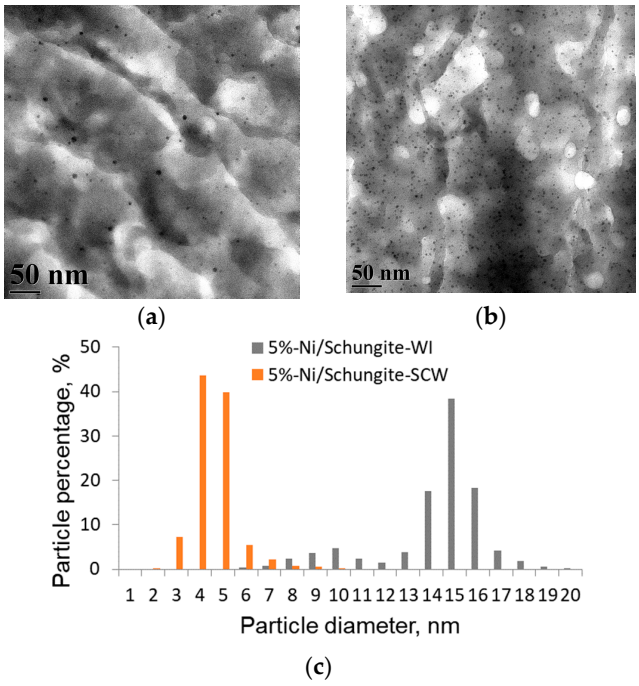

Figure 5. TEM images of the reduced 5%-Ni/schungite-WI (**a**) and 5%-Ni/schungite-SCW (**b**) catalysts, and Ni particle size distribution for both catalysts (**c**).

The comparison of two synthesis methods showed that the precipitation of Ni precursor in subcritical water was more appropriate for obtaining the catalyst with a higher specific surface area and higher dispersion of the Ni-active phase. Further studies were devoted to the catalytic behavior in the deoxygenation of stearic acid.

3.2. Stearic Acid Deoxygenation

n-Hexane was a solvent of choice for the deoxygenation of stearic acid under supercritical conditions, as shown in our previous studies [40,41]. The critical point for n-hexane was at 234.5 °C and has pressure of 3.02 MPa. First, the influence of the catalyst types on the reaction rate and product distribution was investigated. The kinetic curves and the product distribution at close to 100% conversion are presented in Figure 6.

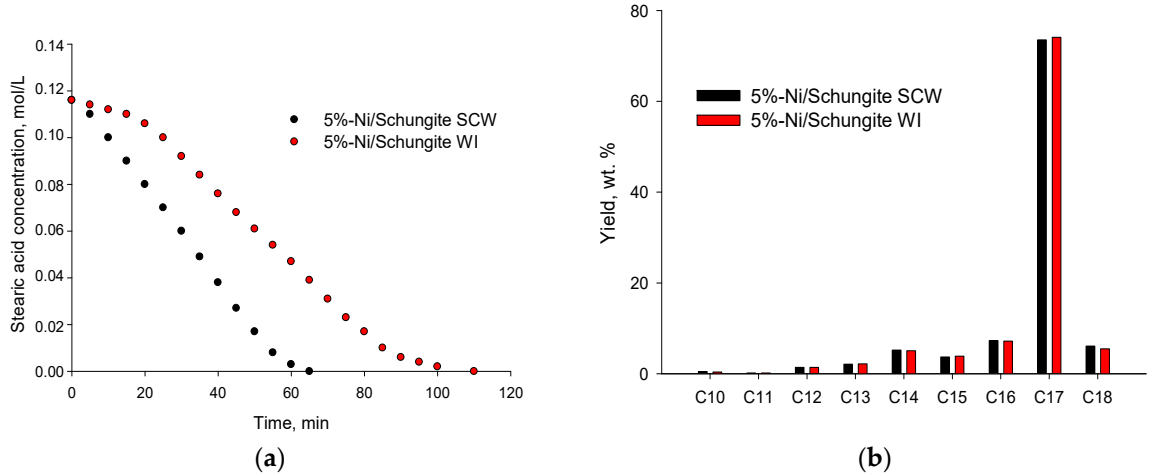

Figure 6. Kinetic curves of stearic acid consumption (**a**) and product yields at 100% conversion of stearic acid (**b**). Process conditions: temperature 280 °C, hydrogen partial pressure 1.5 MPa, and catalyst loading 13.2 mol of stearic acid per mol of Ni.

To compare the catalyst activity, TOF was calculated according to Equation (1).

$$\mathrm{TOF} = \frac{(\mathrm{C(SA)}_0 - \mathrm{C(SA)}_\tau)\cdot \mathrm{V}}{\mathrm{n_{Ni}}\cdot\tau\cdot \mathrm{D}},\ \mathrm{min}^{-1} \quad (1)$$

where $C(SA)_0$ is the initial concentration of stearic acid, mol/L; $C(SA)_\tau$ is the concentration of stearic acid at 50% conversion, mol/L; n_{Ni} is the mol of Ni in the catalyst, mol; τ is the reaction time at 50% conversion, min; D is the Ni dispersion; V is the volume of the reaction mixture, L.

The TOF values were 3.18 min^{-1} for the 5%-Ni/schungite-SCW and 0.54 min^{-1} for 5%-Ni/schungite-WI. The catalyst synthesized by the precipitation in subcritical water was about six times more active in comparison with the one synthesized by wetness impregnation. The TOF values obtained in this study were about 3–6 times higher than those reported in the literature for the same reaction over Ni-containing catalysts [45,46].

The analysis of the kinetic curves (Figure 6a) showed that the stearic acid consumption obeyed a zero-order kinetics (linear dependency "concentration-on-time"), which slowed down at conversions higher than 98%. Such kinetics are typical for the Langmuir–Hinshelwood mechanism with a substrate (stearic acid) strongly adsorbed on the catalyst surface. For the 5%-Ni/schungite-WI catalyst, the kinetic curve had an S-shape with an induction period of 20–25 min, suggesting a catalyst activation in situ during the reaction. This explanation agrees with the TPR profiles (see Figure 4), where the peak maxima for the 5%-Ni/schungite-WI catalyst shifted to the higher temperature (320–330 °C) compared with the 5%-Ni/schungite-SCW sample (290–300 °C).

It is important to underline that both Ni-containing catalysts on the schungite support allowed for stearic acid transformation to alkanes with 100% yield, almost identical product distribution (see Figure 6b), and a yield of n-heptadecane over 70 wt.%. Both catalysts led to the formation of C_{10}–C_{18} alkanes during deoxygenation. The composition of the products indicated preferable decarboxylation with the formation of heptadecanes. However, in supercritical conditions, some cracking was observed, contrary to the "classic" deoxygenation [5,15,17,47–49]. Also, the higher input of cracking should be noted when compared with the Ni-containing catalyst on polymer support [40,41].

As the catalyst synthesized in subcritical water showed a higher activity, further experiments were carried out using the catalysts prepared by this method. To optimize the reaction conditions, the influence of the Ni precursor, Ni concentration in the catalyst, reaction temperature, hydrogen partial pressure, and the substrate-to-catalyst ratio were varied. To study the influence of the Ni precursor salt, the catalysts containing 5 wt.% Ni were synthesized by precipitation in subcritical water using nitrate, acetate, and chloride of nickel. The results of the stearic acid deoxygenation in the presence of the catalysts obtained are presented in Table 3.

Table 3. Influence of the Ni precursor on the activity of the schungite catalysts in stearic acid deoxygenation. Process conditions: temperature 280 °C, hydrogen partial pressure 1.5 MPa, and catalyst loading 13.2 mol of stearic acid per mol of Ni.

Ni Precursor	TOF, min^{-1}	Selectivity to n-Heptadecane, wt.%	Specific Surface Area, m^2/g *	Ni Concentration, wt.% **	Ni Dispersion, % ***
$Ni(NO_3)_2$	3.18 ± 0.01	73.5 ± 0.1	61 ± 2	4.9 ± 0.1	23.4 ± 0.2
$Ni(CH_3COO)_2$	3.05 ± 0.01	73.0 ± 0.1	58 ± 2	4.9 ± 0.1	20.8 ± 0.2
$NiCl_2$	2.48 ± 0.01	72.4 ± 0.1	46 ± 1	4.9 ± 0.1	12.5 ± 0.1

* According to the BET model. ** Ni concentration was estimated by the X-ray fluorescence analysis. *** Ni dispersion was estimated according to CO chemisorption analysis.

The catalysts prepared with nickel nitrate and nickel acetate showed similar activities. Moreover, the Ni dispersion was similar. For the catalyst prepared from nickel chloride, higher aggregation of the active phase was observed, resulting in a decreased dispersion and lower TOF. An increase in particle size in the Ni phase was associated with a decrease in the specific surface area of the catalyst, leading to a 22% decrease in TOF in comparison with the catalyst synthesized from nickel nitrate (see Table 3). The yield of the alkanes as well as the n-heptadecane selectivity were found to be similar for all of the precursors used.

The influence of the Ni concentration in the catalysts on activity/selectivity was studied using the SCW preparation method with nickel nitrate as the precursor. The results of the study are presented in Table 4. The catalyst with a 5 wt.% Ni concentration had the highest activity in terms of TOF value. A decrease in Ni loading to 2 wt.% resulted in decreased TOF. This seems to be due to a longer induction period (activation in situ). The same explanation is valid for the sample with 10 wt.% Ni.

Table 4. Influence of Ni loading on the activity of the schungite-supported catalysts in stearic acid deoxygenation. Process conditions: temperature of 280 °C, hydrogen partial pressure of 1.5 MPa, and catalyst loading 13.2 mol of stearic acid per mol of Ni.

Ni Concentration in Catalyst, wt.% *	TOF, min^{-1}	Selectivity to n-Heptadecane, wt.%	Specific Surface Area, m^2/g **	Ni Dispersion, % ***
2.0 ± 0.1	2.55 ± 0.01	73.8 ± 0.1	65 ± 2	27.6 ± 0.2
4.9 ± 0.1	3.18 ± 0.01	73.5 ± 0.1	61 ± 2	23.4 ± 0.2
9.8 ± 0.1	2.48 ± 0.01	70.2 ± 0.1	39 ± 2	11.2 ± 0.1

* Ni concentration is estimated using the X-ray fluorescence analysis. ** According to the BET model. *** Ni dispersion is estimated according to the CO chemisorption analysis.

The results of the process optimization are presented in Table 5. The experiments were carried out in the presence of a 5%-Ni/schungite-SCW catalyst synthesized using nickel nitrate. The study was performed with temperatures varying from 240 up to 300 °C, hydrogen pressure from 0.5 up to 3.0 MPa, and a substrate–catalyst ratio from 3.3 up to 52.8.

Table 5. Influence of the process parameters on the deoxygenation of stearic acid. Solvent—supercritical n-hexane; catalyst—5%-Ni/schungite-SCW.

Parameter	Value	TOF, min^{-1}	Total Alkane Yield, wt.%	Selectivity to n-Heptadecane, %
Temperature, °C (Process conditions: hydrogen partial pressure of 1.5 MPa, catalyst loading 13.2 mol of stearic acid per mol of Ni)	240	1.76 ± 0.01	81.1 ± 0.1	86.2 ± 0.1
	250	2.18 ± 0.01	89.4 ± 0.1	81.4 ± 0.1
	260	2.52 ± 0.01	95.2 ± 0.1	76.4 ± 0.1
	270	2.87 ± 0.01	98.6 ± 0.1	73.8 ± 0.1
	280	3.18 ± 0.01	99.9 ± 0.1	73.5 ± 0.1
	290	3.75 ± 0.01	99.9 ± 0.1	67.4 ± 0.1
	300	4.23 ± 0.01	99.9 ± 0.1	52.6 ± 0.1
Hydrogen partial pressure, MPa (Process conditions: temperature of 280 °C, catalyst loading 13.2 mol of stearic acid per mol of Ni)	0.5	1.11 ± 0.01	62.4 ± 0.1	92.2 ± 0.1
	1.0	2.38 ± 0.01	79.8 ± 0.1	81.7 ± 0.1
	1.5	3.18 ± 0.01	99.9 ± 0.1	73.5 ± 0.1
	2.0	4.56 ± 0.01	99.9 ± 0.1	72.2 ± 0.1
	2.5	5.48 ± 0.01	99.9 ± 0.1	70.5 ± 0.1
	3.0	6.92 ± 0.01	99.9 ± 0.1	68.7 ± 0.1
Substrate-catalyst ratio, mol stearic acid/mol Ni (Process conditions: temperature of 280 °C, hydrogen partial pressure of 1.5 MPa)	3.3	1.42 ± 0.01	99.9 ± 0.1	51.3 ± 0.1
	6.6	2.23 ± 0.01	99.9 ± 0.1	68.1 ± 0.1
	13.2	3.18 ± 0.01	99.9 ± 0.1	73.5 ± 0.1
	26.4	5.06 ± 0.01	88.1 ± 0.1	86.4 ± 0.1
	52.8	7.25 ± 0.01	76.4 ± 0.1	98.5 ± 0.1

An increase in deoxygenation temperature from 240 up to 300 °C led to an increase in the total yield of alkanes, but decreased the selectivity towards n-heptadecane. At temperatures below 270 °C, a high concentration of aldehydes and alcohols was observed in the reaction products, indicating that the process went through hydrodeoxygenation. An increase in temperature accelerated the decarbonylation and decarboxylation reactions, but the cracking processes also decreased the carbon number of the alkanes formed at an accelerated pace. The temperature dependence allowed for calculating the apparent activation energy of the deoxygenation of stearic acid carried out in supercritical conditions, which was found to be 34 ± 0.5 kJ/mol. This value was slightly lower than the one for the "classic" deoxygenation (40–120 kJ/mol) [5,11,17,21,25].

The yield of alkanes increased while increasing the partial hydrogen pressure from 0.5 to 3.0 MPa. However, the n-heptane selectivity decreased significantly in the pressure range of 0.5–1.5 MPa. The further increase in hydrogen pressure led to a slight acceleration of cracking processes, resulting in the formation of alkanes with a carbon number of 10–15. Similar results were observed when decreasing the substrate–catalyst ratio. At high concentrations of stearic acid, the yield of alkanes decreased, and the formation of alcohols and aldehydes was observed. A decrease in the stearic acid concentration led to a rise of the total alkane yield, but a decrease in the concentration of n-heptadecane. The reaction order with respect to hydrogen was found to be 1, and with respect to the stearic acid it was calculated to be 0.5 under the conditions applied.

In summary, the optimal conditions for stearic acid deoxygenation were the following: the solvent is supercritical n-hexane, catalyst is 5%-Ni/schungite-SCW, temperature is 280 °C, hydrogen partial pressure is 1.5 MPa, and catalyst loading is 13.2 mol of stearic acid per mol of Ni. Under these optimal process conditions, the catalyst stability was tested by consecutive reaction runs. Before each cycle, the catalyst was washed with n-hexane without any supplemental treatment. The catalyst was shown to be stable in terms of activity and selectivity during 15 cycles (see Figure 7).

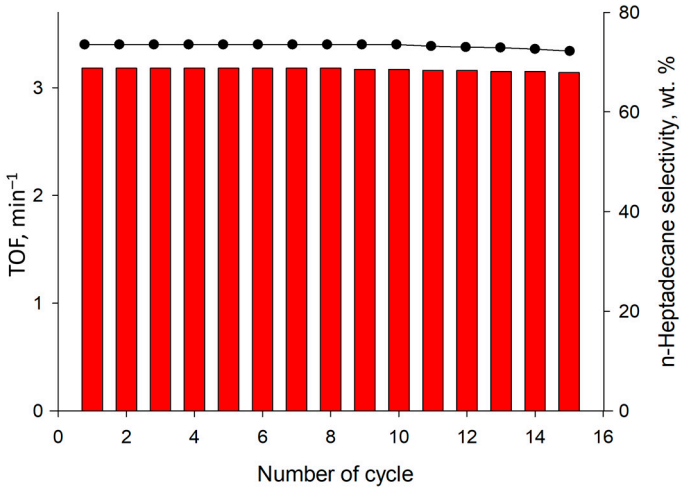

Figure 7. Stability test for the 5%-Ni/schungite-SCW. Process conditions: temperature 280 °C, hydrogen partial pressure of 1.5 MPa, catalyst loading of 13.2 mol of stearic acid per mol of Ni.

4. Conclusions

Green diesel produced from biomass via deoxygenation is a valuable alternative to replace petroleum-derived diesel. The success and cost-effectiveness of biomass processing rely on the active/stable catalyst and optimized reaction conditions. Significant intensification of deoxygenation can be achieved under supercritical conditions due to reduced mass-transfer limitations, leading to increased transformation rate.

In this work, an in-depth study of the stearic acid deoxygenation in n-hexane as a solvent was carried out under supercritical conditions. Novel Ni-containing catalysts based on carbon-mineral support, schungite, were developed. Schungite is an inexpensive natural adsorbent that demonstrates a significant adsorption capacity for organics and a high mechanical strength. The series of Ni-supported on schungite were obtained by precipitation in subcritical water and, for comparison, via conventional wetness impregnation. In both cases, the catalysts were followed by calcination at 500 °C and reduction in hydrogen flow at 300 °C. The catalysts were thoroughly characterized to determine their SSA, porosity, crystallinity, composition, thermostability, and dispersion of the active phase. The schungite support and the catalysts demonstrated a high mechanical strength and thermal stability during their synthesis (precursor deposition in subcritical water, calcination, and reduction) and in the catalytic testing. The catalyst synthesized by hydrothermal deposition of Ni showed a three-fold higher specific surface area compared with the catalysts synthesized via conventional wetness impregnation. Moreover, the active phase deposited hydrothermally was more evenly distributed through the support with an almost three times smaller mean particle size of Ni (ca. 4.5 nm) as compared to the impregnated ones. The catalytic activity was tested for stearic acid deoxygenation (model of green diesel from biomass) in n-hexane under supercritical conditions. The catalyst demonstrated a six-fold increase in the rate of transformation for the samples synthesized by the SCW method. Under optimal process conditions, full conversion of the stearic acid was obtained for 60 min with close to 100% yield of C_{10}–C_{18} alkanes containing over 70 wt.% of targeted n-heptadecane. The catalyst reuse in 15 consecutive reaction runs confirmed its stability.

Supplementary Materials: The following supporting information can be downloaded at: https://www.mdpi.com/article/10.3390/pr12071503/s1. Figure S1: Scheme of catalyst synthesis via wetness impregnation. Figure S2: Scheme of setup for catalyst synthesis via precipitation in subcritical water: 1—reactor, 2—thermostate, 3—thermocouple, 4—stirrer rotor, 5—controller, 6—balloon with nitrogen, 7—manometer. Figure S3: Scheme of catalyst synthesis via precipitation in subcritical water. Figure S4: Scheme of setup for stearic acid deoxygenation: 1—main block, 2—power switch, 3—stirrer regulator, 4—reactor, 5—blow connection, 6—sampler, 7—thermocouple, 8—manometer, 9—gas supplying controller, 10—reductor. Figure S5: FTIR spectra of the samples: (a) schungite,

(b) 5%-Ni/schungite-WI as prepared, (c) 5%-Ni/schungite-SCW as prepared, (d) 5%-Ni/schungite-SCW calcined.

Author Contributions: Conceptualization, L.K.-M. and A.A.S.; methodology, A.I.S., M.G.S.; investigation, E.O.S., M.E.M. and A.V.B.; writing—original draft preparation, E.O.S.; writing—review and editing, A.A.S. and L.K.-M.; project administration, A.A.S.; validation, V.G.M. All authors have read and agreed to the published version of the manuscript.

Funding: This research was funded by the Russian Science Foundation, grant number 22-79-10096.

Data Availability Statement: Data are contained within the article and Supplementary Materials.

Acknowledgments: We thank Yury V. Lugovoy (Department of biotechnology, chemistry and standardization, Tver State Technical University, A. Nikitin Str., 22, 170026 Tver, Russia) for the help in thermogrvimetric analysis.

Conflicts of Interest: The authors declare no conflicts of interest.

References

1. Asikin-Mijan, N.; Juan, J.C.; Taufiq-Yap, Y.H.; Ong, H.C.; Lin, Y.C.; AbdulKareem-Alsultan, G.; Lee, H.V. Towards sustainable green diesel fuel production: Advancements and opportunities in acid-base catalyzed H_2-free deoxygenation process. *Catal. Commun.* **2023**, *182*, 106741. [CrossRef]
2. Belousov, A.S.; Esipovich, A.L.; Kanakov, E.A.; Otopkova, K.V. Recent advances in sustainable production and catalytic transformations of fatty acid methyl esters. *Sustain. Energy Fuels* **2021**, *5*, 4512–4545. [CrossRef]
3. Barbosa, I.V.; Scapim, L.A.; Cavalcante, R.M.; Young, A.F. Industrial production of green diesel in Brazil: Process simulation and economic perspectives. *Renew. Energy* **2023**, *219*, 119591. [CrossRef]
4. Sonthalia, A.; Kumar, N. Hydroprocessed vegetable oil as a fuel for transportation sector: A review. *J. Energy Inst.* **2019**, *92*, 1–17. [CrossRef]
5. Amin, A. Review of diesel production from renewable resources: Catalysis, process kinetics and technologies. *Ain Shams Eng. J.* **2019**, *10*, 821–839. [CrossRef]
6. Cremonez, P.A.; Teleken, J.G.; Weiser Meier, T. Potential of green diesel to complement the Brazilian energy production: A review. *Energy Fuels* **2021**, *35*, 176–186. [CrossRef]
7. Azman, N.S.; Marliza, T.S.; Mijan, N.A.; Yun Hin, T.Y.; Khairuddin, N. Production of Biodiesel from Waste Cooking Oil via Deoxygenation Using Ni-Mo/Ac Catalyst. *Processes* **2021**, *9*, 750. [CrossRef]
8. Alvarez-Galvan, M.C.; Blanko-Brieva, G.; Capel-Sanchez, M.; Morales-delaRosa, S.; Campos-Martin, J.M.; Fierro, J.L.G. Metal phosphide catalysts for the hydrotreatment of non-edible vegetable oils. *Catal. Today* **2018**, *302*, 242–249. [CrossRef]
9. Ameen, M.; Azizan, M.T.; Yusup, S.; Ramli, A.; Shahbaz, M.; Aqsha, A. Process optimization of green diesel selectivity and understanding of reaction intermediates. *Renew. Energy* **2020**, *149*, 1092–1106. [CrossRef]
10. Sousa, F.P.; Silva, L.N.; de Rezende, D.B.; de Oliveira, L.C.; Pasa, V.M.D. Simultaneous deoxygenation, cracking and isomerization of palm kernel oil and palm olein over beta zeolite to produce biogasoline, green diesel and biojet-fuel. *Fuel* **2018**, *223*, 149–156. [CrossRef]
11. Oi, L.E.; Choo, M.Y.; Lee, H.V.; Taufiq-Yap, Y.H.; Cheng, C.K.; Juan, J.C. Catalytic deoxygenation of triolein to green fuel over mesoporous TiO_2 aided by in situ hydrogen production. *Int. J. Hydrog. Energy* **2020**, *45*, 11605–11614. [CrossRef]
12. Manimaran, R.; Mohanraj, T.; Prabakaran, S. Biodegradable waste-derived biodiesel as a potential green fuel: Optimization of production process and its application in diesel engine. *Ind. Crops Prod.* **2023**, *192*, 116078. [CrossRef]
13. Cavalcanti, C.D.S.; Ravagnani, M.A.S.S.; Stragevitch, L.; Carvalho, F.R.; Pimentel, M.F. Simulation of the soybean oil hydrotreating process for green diesel production. *Clean. Chem. Eng.* **2022**, *1*, 100004. [CrossRef]
14. Ayala-Cortes, A.; Torres, D.; Frecha, E.; Arcelus-Arrillaga, P.; Villafan-Vidales, H.I.; Langoria, A.; Pinilla, J.L.; Suelves, I. Upgrading of biomass-derived solar hydrothermal bio-oils through catalytic hydrodeoxygenation in supercritical ethanol. *J. Environ. Chem. Eng.* **2023**, *11*, 111395. [CrossRef]
15. Zamani, A.S.; Saidi, M.; Najafabadi, A.T. Selective production of diesel-like alkanes via Neem seed oil hydrodeoxygenation over $Ni/MgSiO_3$ catalyst. *Renew. Energy* **2023**, *209*, 462–470. [CrossRef]
16. Jeon, K.W.; Gong, J.H.; Kim, M.J.; Shim, J.O.; Jang, W.J.; Roh, H.S. Review on the production of renewable biofuel: Solvent-free deoxygenation. *Renew. Sustain. Energy Rev.* **2024**, *195*, 114325. [CrossRef]
17. Mahene, W.L.; Kivevele, T.; Machunda, R. The role of textural properties and surface chemistry of activated carbon support in catalytic deoxygenation of triglycerides into renewable diesel. *Catal. Commun.* **2023**, *181*, 106737. [CrossRef]
18. Liu, X.; Guo, Y.; Xu, D.; Guan, Q. A review on recent advances in clean microalgal bio-oil production via catalytic hydrothermal deoxygenation. *J. Clean. Prod.* **2022**, *366*, 132978. [CrossRef]
19. Konwar, L.J.; Mikkola, J.P. Carbon support effects on metal (Pd, Pt and Ru) catalyzed hydrothermal decarboxylation/deoxygenation of triglycerides. *Appl. Catal. A Gen.* **2022**, *638*, 118611. [CrossRef]

20. Zhang, Z.; Okejiri, F.; Li, Y.; Li, J.; Fu, J. Hydrodecarboxylation of Fatty Acids into Liquid Hydrocarbons over Commercial Ru/C Catalyst under Mild Conditions. *New J. Chem.* **2020**, *44*, 7642–7646. [CrossRef]
21. Omer, A.; Kazmi, W.W.; Rahimipetroudi, I.; Syed, M.W.; Rashid, K.; Yang, J.B.; Lee, I.G.; Dong, S.K. Experimental and numerical study on the hexadecanoic acid upgrading kinetics under supercritical ethanol without the use of hydrogen. *Renew. Energy* **2023**, *2019*, 119552. [CrossRef]
22. Lin, M.; Yan, Y.; Li, X.; Li, R.; Wu, Y. Potassium-assisted activation strategy regulating metal-support interaction to promote hydrothermal hydrogenation/deoxygenation of palmitic acid. *Fuel Process. Technol.* **2023**, *250*, 107892. [CrossRef]
23. Baharudin, K.B.; Taufiq-Yap, Y.H.; Hunns, J.; Isaacs, M.; Wilson, K.; Derawi, D. Mesoporous NiO/Al-SBA-15 catalysts for solvent-free deoxygenation of palm fatty acid distillate. *Microporous Mesoporous Mater.* **2019**, *276*, 13–22. [CrossRef]
24. Li, X.; Li, R.; Lin, M.; Yang, M.; Wu, Y. High hydrothermal stability Co@NC catalyst for hydrothermal deoxygenation of algae-based bio-oil model compound. *Chem. Eng. Sci.* **2024**, *284*, 119450. [CrossRef]
25. Gamal, M.S.; Asikin-Mijan, N.; Khalit, W.N.A.W.; Arumugam, M.; Izham, S.M.; Taufiq-Yap, Y.H. Effective catalytic deoxygenation of palm fatty acid distillate for green diesel production under hydrogen-free atmosphere over bimetallic catalyst CoMo supported on activated carbon. *Fuel Process. Technol.* **2020**, *208*, 106519. [CrossRef]
26. Papageridis, K.N.; Charisiou, N.D.; Douvartzides, S.; Sebastian, V.; Hinder, S.J.; Baker, M.A.; AlKhoori, A.A.; Alkhoori, S.I.; Polychronopoulou, K.; Goula, M.A. Continuous selective deoxygenation of palm oil for renewable diesel production over Ni catalysts supported on Al_2O_3 and La_2O_3–Al_2O_3. *RSC Adv.* **2021**, *11*, 8569. [CrossRef]
27. Mahdi, H.I.; Bazargan, A.; McKay, G.; Azelee, N.I.W.; Meili, L. Catalytic deoxygenation of palm oil and its residue in green diesel production: A current technological review. *Chem. Eng. Res. Des.* **2021**, *174*, 158–187. [CrossRef]
28. Chean, K.W.; Yusup, S.; Loy, A.C.M.; How, B.S.; Skoulou, V.; Taylor, M.J. Recent advances in the catalytic deoxygenation of plant oils and prototypical fatty acid models compounds: Catalysis, process, and kinetics. *Mol. Catal.* **2022**, *523*, 111469.
29. Luo, W.; Cao, W.; Bruijnincx, P.C.A.; Lin, L.; Wang, A.; Zhang, T. Zeolite-supported metal catalysts for selective hydrodeoxygenation of biomass-derived platform molecules. *Green Chem.* **2019**, *21*, 3744. [CrossRef]
30. Obradovic, N.; Gigov, M.; Dordevic, A.; Kern, F.; Dmitrovic, S.; Matovic, B.; Dordevic, A.; Tshantshapanyan, A.; Vlanovic, B.; Petrovic, P.; et al. Shungite—A carbon-mineral rock material: Its sinterability and possible applications. *Process. Appl. Ceram.* **2019**, *13*, 89–97. [CrossRef]
31. Rozhkova, N.N. Schungite Nanocarbons: Structural and Physics Chemical Properties, Activation Mechanisms. Ph.D. Thesis, Institute of Geology, Karelian Science Center, RAS, Saint-Petersburg, Russia, 2013; p. 39.
32. Frac, M.; Szudek, W.; Szoldra, P.; Pichor, W. The applicability of shungite as an electrically conductive additive in cement composites. *J. Build. Eng.* **2022**, *45*, 103469. [CrossRef]
33. Efremov, S.; Nachiporenko, S.; Tokmurzin, D.; Kaiaidarova, A.; Kalugin, S.; Tassibekov, K. Remediation of soil contaminated by toxic rocket fuel components using modified carbon–mineral adsorbing material produced from shungite rock modified with Mn^{4+} and Fe^{3+}. *Environ. Technol. Innov.* **2021**, *24*, 101962. [CrossRef]
34. Mooste, M.; Tkesheliadze, T.; Kozlova, J.; Kikas, A.; Kisand, V.; Treshchalov, A.; Tamm, A.; Aruvali, J.; Zagal, J.H.; Kannan, A.M.; et al. Transition metal phthalocyanine-modified shungite-based cathode catalysts for alkaline membrane fuel cell. *Int. J. Hydrog. Energy* **2021**, *46*, 4365–4377. [CrossRef]
35. Balta, Z.; Simsek, E.B. Insights into the photocatalytic behavior of carbon-rich shungite-based WO_3/TiO_2 catalysts for enhanced dye and pharmaceutical degradation. *New Carbon. Mater.* **2020**, *35*, 371–383. [CrossRef]
36. Stepacheva, A.A.; Markova, M.E.; Schipanskaya, E.O.; Matveeva, V.G.; Sulman, M.G. Highly Effective Schungite-Based Catalyst for Deoxygenation of Biomass Components. *Chem. Eng. Trans.* **2021**, *88*, 283–288.
37. Thommes, M.; Kaneko, K.; Neimark, A.V.; Olivier, J.P.; Rodrigues-Reinoso, F.; Rouquerol, J.; Sing, K.W. Physisorption of Gases, with Special Reference to the Evaluation of Surface Area and Pore Size Distribution (IUPAC Technical Report). *Pure Appl. Chem.* **2015**, *87*, 1051–1069. [CrossRef]
38. He, X.; Xu, Y.; Yao, X.; Zhang, C.; Pu, Y.; Wang, X.; Mao, W.; Du, Y.; Zhong, W. Large exchange bias and enhanced coercivity in strongly-coupled Ni/NiO binary nanoparticles. *RSC Adv.* **2019**, *9*, 30195–30206. [CrossRef] [PubMed]
39. Yin, W.; Venderbosch, R.H.; He, S.; Bykova, M.V.; Khromova, S.A.; Yakovlev, V.A.; Heeres, H.J. Mono-, bi-, and tri-metallic Ni-based catalysts for the catalytic hydrotreatment of pyrolysis liquids. *Biomass-Convers. Biorefinery* **2017**, *7*, 361–376. [CrossRef]
40. Stepacheva, A.A.; Sidorov, A.I.; Matveeva, V.G.; Sulman, E.M.; Sulman, M.G. Synthesis Fatty acid deoxygenation in supercritical hexane over catalysts synthesized hydrothermally for biodiesel production. *Chem. Eng. Technol.* **2019**, *42*, 780–787. [CrossRef]
41. Stepacheva, A.A.; Bykov, A.V.; Sidorov, A.I.; Sulman, M.G.; Matveeva, V.G.; Sulman, E.M.; Markova, M.E. Ni catalyst synthesized by hydrothermal deposition on the polymer matrix in the supercritical deoxygenation of fatty acids. *React. Kinet. Mech. Catal.* **2018**, *13*, 74–81.
42. Zhang, Z.; Zhao, G.; Sun, W.; Liu, Y.; Lu, Y. Oxidative Dehydrogenation of Ethane: Superior Nb_2O_5-NiO/Ni-Foam Catalyst Tailored by Tuning Morphology of NiO-Precursors Grown on a Ni-Foam. *iScience* **2019**, *20*, 90–99. [CrossRef] [PubMed]
43. De, S.; Zhang, J.; Luque, R.; Yan, N. Ni-based bimetallic heterogeneous catalysts for energy and environmental applications. *Energy Environ. Sci.* **2016**, *9*, 3314–3347. [CrossRef]
44. L'vov, B.V.; Galwey, A.K. The mechanism and kinetics of NiO reduction by hydrogen. Thermochemical approach. *J. Therm. Anal. Calorim.* **2012**, *110*, 601–610. [CrossRef]

45. Lin, M.; Yan, Y.; Li, X.; Li, R.; Wu, Y. Hydrothermal hydrogenation/deoxygenation of palmitic acid to alkanes over Ni/activated carbon catalyst. *Chin. J. Chem. Eng.* **2024**, *66*, 8–18. [CrossRef]
46. Liu, Y.; Xheng, D.; Yu, H.; Liu, X.; Yu, S.; Wang, X.; Li, L.; Pang, J.; Liu, X.; Yan, Z. Rapid and green synthesis of SAPO-11 for deoxygenation of stearic acid to produce bio-diesel fractions. *Microporous Mesoporous Mater.* **2020**, *303*, 110280. [CrossRef]
47. Jeon, K.W.; Park, H.R.; Lee, Y.L.; Kim, J.E.; Jang, W.J.; Shim, J.O.; Roh, H.S. Deoxygenation of non-edible fatty acid for green diesel production: Effect of metal loading amount over Ni/MgO–Al_2O_3 on the catalytic performance and reaction pathway. *Fuel* **2022**, *311*, 122488. [CrossRef]
48. Hongloi, N.; Prapainainar, P.; Prapainainar, C. Review of green diesel production from fatty acid deoxygenation over Ni-based catalysts. *Mol. Catal.* **2022**, *523*, 111696. [CrossRef]
49. Tsiotsias, A.I.; Hafeez, S.; Charisiou, N.D.; Al-Salem, S.M.; Manos, G.; Constantinou, A.; Alkhoori, S.; Sebastian, V.; Hinder, S.J.; Baker, M.A.; et al. Selective catalytic deoxygenation of palm oil to produce green diesel over Ni catalysts supported on ZrO_2 and CeO_2–ZrO_2: Experimental and process simulation modelling studies. *Renew. Energy* **2023**, *206*, 582–596. [CrossRef]